Photonics and Nanostructures – Fundamentals and Applications 28 (2018) 37–44

Contents lists available at ScienceDirect

Photonics and Nanostructures – Fundamentals and Applications

journal homepage: www.elsevier.com/locate/photonics

Angle-resolved reflection spectroscopy of high-quality PMMA opal crystal

Ivan V. Nemtsev[a,b,*], Igor A. Tambasov[b], Alexander A. Ivanenko[b], Victor Ya. Zyryanov[b]

[a] Federal Research Centre Krasnoyarsk Scientific Center of the Siberian Branch of Russian Academy of Sciences, Akademgorodok 50, 660036 Krasnoyarsk, Russia

[b] Kirensky Institute of Physics, Federal Research Centre Krasnoyarsk Scientific Center of the Siberian Branch of Russian Academy of Sciences, Akademgorodok 50, 660036 Krasnoyarsk, Russia

ARTICLE INFO

Article history:
Received 13 September 2017
Received in revised form 9 November 2017
Accepted 20 November 2017
Available online 23 November 2017

Keywords:
PMMA opal
Photonic crystal
Electron microscopy
Angular resolved reflective spectroscopy

ABSTRACT

PMMA opal crystal was prepared by a simple hybrid method, which includes sedimentation, meniscus formation and evaporation. We investigated three surfaces of this crystal by angle-resolved reflective light spectroscopy and SEM study. The angle-resolved reflective measurements were carried out in the 400–1100 nm range. We have determined the high-quality ordered surface of the crystal region. Narrow particle size distribution of the surface has been revealed. The average particle diameter obtained with SEM was nearly 361 nm. The most interesting result was that reflectivity of the surface turned out up to 98% at normal light incidence. Using a fit of dependences of the maximum reflectivity wavelength from an angle based on the Bragg–Snell law, the wavelength of maximum 0° reflectivity, the particle diameter and the fill factor have been determined. For the best surface maximum reflectivity wavelength of a 0° angle was estimated to be 869 nm. The particle diameter and fill factor were calculated as 372 nm and 0.8715, respectively. The diameter obtained by fitting is in excellent agreement with the particle diameter obtained with SEM. The reflectivity maximum is assumed to increase significantly when increasing the fill factor. We believe that using our simple approach to manufacture PMMA opal crystals will significantly increase the fabrication of high-quality photonic crystal templates and thin films.

1. Introduction

Photonic crystals (PhCs) are attractive optical materials for fundamental research and practical applications in various fields of technology due to their outstanding properties. Among these properties the photon stop-band (or photonic band gap, PBG), light-wavelength selectivity and high-performance photoluminescence are of primary importance [1–8].

Structural periodicity in a PhC leads to light coherent scattering from a highly accurate, ordered structure that results in the formation of PBGs, which are optical analogues of electronic band gaps in semiconductors [9]. The PBG is known to be in agreement with light reflection from a periodic structure if the structure period is equal to half of the incident light wavelength [10]. Moreover, wavelength selectivity [4] and total reflection [11] take place entirely due to PhC periodic order.

PhCs have worldwide been investigated for their possible application in biological labeling [12,13], therapeutics [14,15], biodetection [15], bioimaging [15,16] and solar cells [17,18]. Based on their promising properties infrared quantum counter detectors, temperature sensors and three-dimensional displays [19] are feasible. There are some more attractive phenomena concerning PhCs, such as extraordinary optical transmission [20], low-loss transmission [21], enhanced absorption [22,23] and multi-functional and multi-responsive luminescence [24]. Some PhC devices are already in use. For example, PhC fibers [25], LED [26], no-loss waveguides [27,28], resonators [29] and compact solid-state lasers [30] have already been fabricated.

Among PhCs, opals (natural or artificial) are distinguished as a special class. Opals are three-dimensional periodic crystals of great interest [31], which derives from the fact that opals can be prepared using relatively simple and inexpensive production methods, and considerable surface area of three-dimensional, highly precise, ordered templates of opal can also be obtained. Obviously the most appropriate technique to fabricate colloidal crystal is the

* Corresponding author at: Federal Research Centre Krasnoyarsk Scientific Center of the Siberian Branch of Russian Academy of Sciences, Akademgorodok 50, Krasnoyarsk, 660036, Russia.
E-mail address: ivan_nemtsev@mail.ru (I.V. Nemtsev).

https://doi.org/10.1016/j.photonics.2017.11.007
1569-4410/

self-assembly approach [31], the most popular methods of which are gravity sedimentation, vertical deposition, electrophoresis, spin coating as well as the melt-shear organization technique [32,33] and crystallization in physically confined cells [31]. Nowadays a number of researchers [34–37] have concentrated on combining stimulus-responsive materials with the self-assembled PhCs.

Inverted or inverse opals (IOs) are a particular case of PhCs [38–40], commonly used in gas and liquid sensing [41–43], battery electrodes [44] and catalysts [45–47]. More recently, a series of works [48–50] have been devoted to so-called smart devices based on inverted opal structures. IOs are three-dimensional porous structures formed using sacrificial polymer[24] or silica [51] templates by filling the opal voids with a precursor. The original opal template is then removed by etching or annealing. As a polymer template, polymethyl methacrylate (PMMA) or polystyrene opal is conveniently used. To obtain a high-quality inverse opal, the most-ordered PMMA or polystyrene spheres in the opal template should be fabricated.

One of the main methods to check opal template quality is optical reflection and scanning electron microscopy (SEM). The reflection at normal incident light for an ideal opal template is 100% under certain wavelengths. Indeed, research works have confirmed high opal template reflectivity [3,52–54]. However, no studies have been identified in which the opal crystal reflectivity reaches 100% from a relatively large area. An analysis of articles on this topic showed that the highest reflectivity from a relatively large area of opal crystal was ~ 80% measured with incident light normal to the *hkl* = 111 crystal planes [55]. Thus, the purpose of this study was to produce a high-quality opal crystal with reflectivity reaching 100% from a relatively large area by using a simple and inexpensive method.

This study presents a high-quality opal surface with extrapolated reflectivity up to 98% at normal incidence, as well as bulk opal made from stacking uniform-sized particles into a face-centre cubic (fcc) array. The opal crystal was produced using a hybrid method, which includes sedimentation, meniscus formation and evaporation. This method is simple and allows relatively large high-ordered surfaces with high reflection. We have found that our hybrid method is similar to the methods specified in recent research [55,56]. However, different technological parameters were used here.

This study presents angle-resolved reflective measurements and an SEM study of opal PMMA crystal with three surfaces.

2. Experiment

2.1. Synthesis of PMMA spheres

Methyl methacrylate (MMA), distilled water and 2,2′-Azobis(2-methylpropionamidine) dihydrochloride initiator were used for synthesis of the PMMA emulsion. A necessary condition of the dispersion formation of submicron PMMA spheres with a narrow size distribution is a short phase of intense multiple nucleation, changing with slow controlled growth of the particles without changing their numbers. The chain radical polymerization process of methyl methacrylate can be divided into three stages: activation of the initiator, the reaction of the monomer with an initiator radical and the growth of the molecule and breakage of the polymer chain. When heated, the initiator decomposes with the formation of active radicals, which are the initiators of the polymerization reaction.

The emulsion polymerization procedure requires the heating of methyl methacrylate emulsified in water to 70 °C or 80 °C. In this study, the emulsion temperature was kept at 75 °C. We used 140 ml of MMA, 560 ml of distilled water and 0.3 g of initiator to make PMMA spheres of 360–370 nm. The mixer speed was fixed at 700 rpm. All polymerization procedures for mixing water and methyl methacrylate lasted about 2.5 h. During nanoparticle (NP) dispersion synthesizing, the IR spectra of the NP dispersion was recorded by using a FT-801 IR Fourier spectrometer with a fibre probe [57]. Thus, we were able to fully monitor the polymerization process using IR spectra. Before polymerization, we saw only MMA peaks. However, after the polymerization process, we saw only PMMA peaks. Peaks of MMA and PMMA were identified using the following articles [58–60]. Thus, we assume that all chemical reagents completely reacted.

The concentration of nanoparticles in water dispersion was estimated to be ~15 vol% (~6×10^{15} nanoparticles per one liter). The polydispersity of the nanoparticles was less than 3% according to SEM.

2.2. Preparation of PMMA opal-like structure

In this study, we used the hybrid method to form opal PMMA crystals. This hybrid method included sedimentation, meniscus formation and evaporation. Our method is slightly similar to Colvin's one [61], but there are a wide range of differences: materials of colloidal particles, cavities for crystallization, evaporation and sedimentation conditions, sample sizes. Hot emulsion of PMMA spheres was poured in a small bowl coated with polytetrafluoroethylene, which has hydrophobicity. Recent studies have shown that hydrophobicity plays a key role in the formation of high-quality opal crystals [55,56,62]. The bowl volume was near 100 ml, the diameter was 90 mm and the rounding radius between the bottom and the wall of the bowl was approximately 13 mm (meniscus-like area).

During opal manufacturing, the bowl was not covered and kept at room temperature. In addition, there was no shaking of the bowl with the emulsion. We waited 350 h until the water in the bowl was completely naturally evaporated. The humidity in the room was constant at 60%. Finally, the opal crystal was obtained. Thus, the use of a hydrophobic surface and a long duration of self-assembly led to the formation of an opal crystal with a high-quality surface.

2.3. Apparatus and analytical conditions

The FTIR-spectra were performed with a VERTEX 80 V spectrometer equipped with an A513 variable angle reflection accessory. The FTIR-spectra were obtained in 25000–8000 cm^{-1} with resolution 2 cm^{-1}. Morphology analysis was carried out with a Hitachi S-5500 field emission scanning electron microscope (FE-SEM) at 3 kV using secondary electron imaging. No metal films were coated on the sample surface prior to taking the SEM measurement in case of a dielectric sample. During deposition, sputter coater damages every polymer sphere and opal-like structure. That is why surface charging occurs despite using the charge suppression scan mode of the SEM.

3. Results and discussion

A bulk colloidal crystal with a high-quality surface was grown. A segment was taken from the colloidal crystal centre as shown in Fig. 1a. Places where samples were taken are shown in Fig. 1b.

Fig. 2 shows the SEM study of three surface types marked as Samples 1, 2 and 3. Sample 1 is the part of the bulk opal corresponding the bowl-opal interface. Sample 2 is obtained from a direct meniscus (sample-air interface). Sample 3 is the middle-part of the opal crystal (sample-air interface).

As shown in Fig. 2a, there is a short-range order in Sample 1, but disorder is mainly observed. The inset in the top right corner of Fig. 2a demonstrates that no ideal spheres are observed. Fig. 2b shows that there is a long-range order with high-ordered polymer

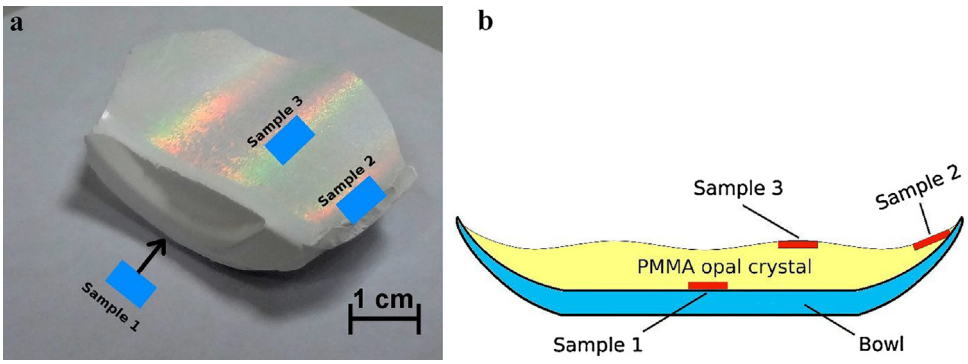

Fig. 1. The photo of the middle of the PMMA bulk opal crystal **(a)** and the scheme where the samples were taken from the opal crystal **(b)**.

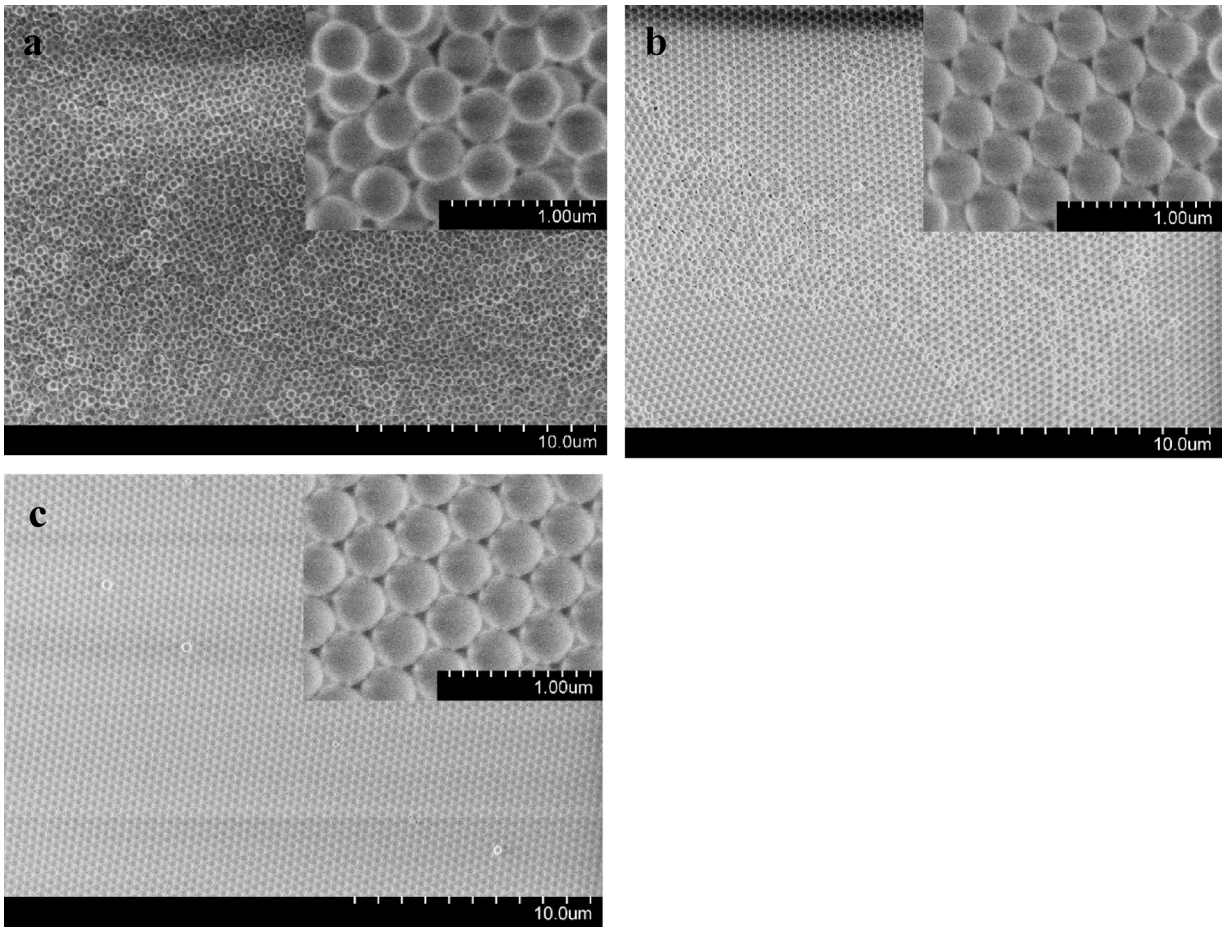

Fig. 2. SEM micrographs of the three different surfaces: surface of Sample 1 **(a)**, surface of Sample 2 **(b)** and surface of Sample 3 **(c)**.

spheres. Some domains, domain walls and vacancies are also visible in Fig. 2b. In the inset of Fig. 2b, a good order of spheres is visible. Sample 3 has the best structure as shown in Fig. 2c and its inset. There is a long-range order of perfectly-ordered spheres. There appear to be no domains in Sample 3.

To estimate the particle size distributions, we made a distribution histogram for Sample 1, Sample 2 and Sample 3. The distribution histogram was built as follows. From each Fig. 2a–c 100 particles were taken. The diameter of each particle was determined using GIMP program. This program allows to measure scale bars as well as particle sizes in pixels. Since we know the scale bar length in nanometres, we estimated PMMA particle sizes in nanometres using the pixel-to-nanometre ratio. We built the distribution histogram and determined the mean diameter for each sample by using OriginPro: $D_{Sample3} = 361 \pm 6.62$ nm; $D_{Sample2} = 372 \pm 4.50$ nm; $D_{Sample1} = 377 \pm 4.66$ nm. Fig. 3 demonstrates the distribution of PMMA spheres for each sample. The particle-size dispersity is no more than 14 nm; relatively, the mean value corresponds to less than 4% deviation.

It is probable that larger particles settle faster than smaller particles if we assume that larger particles are heavier than smaller particles. Therefore, we see these particles in Sample 1. We can see the mean size in the meniscus-like area, where it is likely that the process of sedimentation of larger particles is associated with the process of sedimentation of smaller particles However, smaller particles are easier so they swim for a longer time comparison with larger particles. Thus, it is possible that these smaller particles are located closer to the surface on Sample 3.

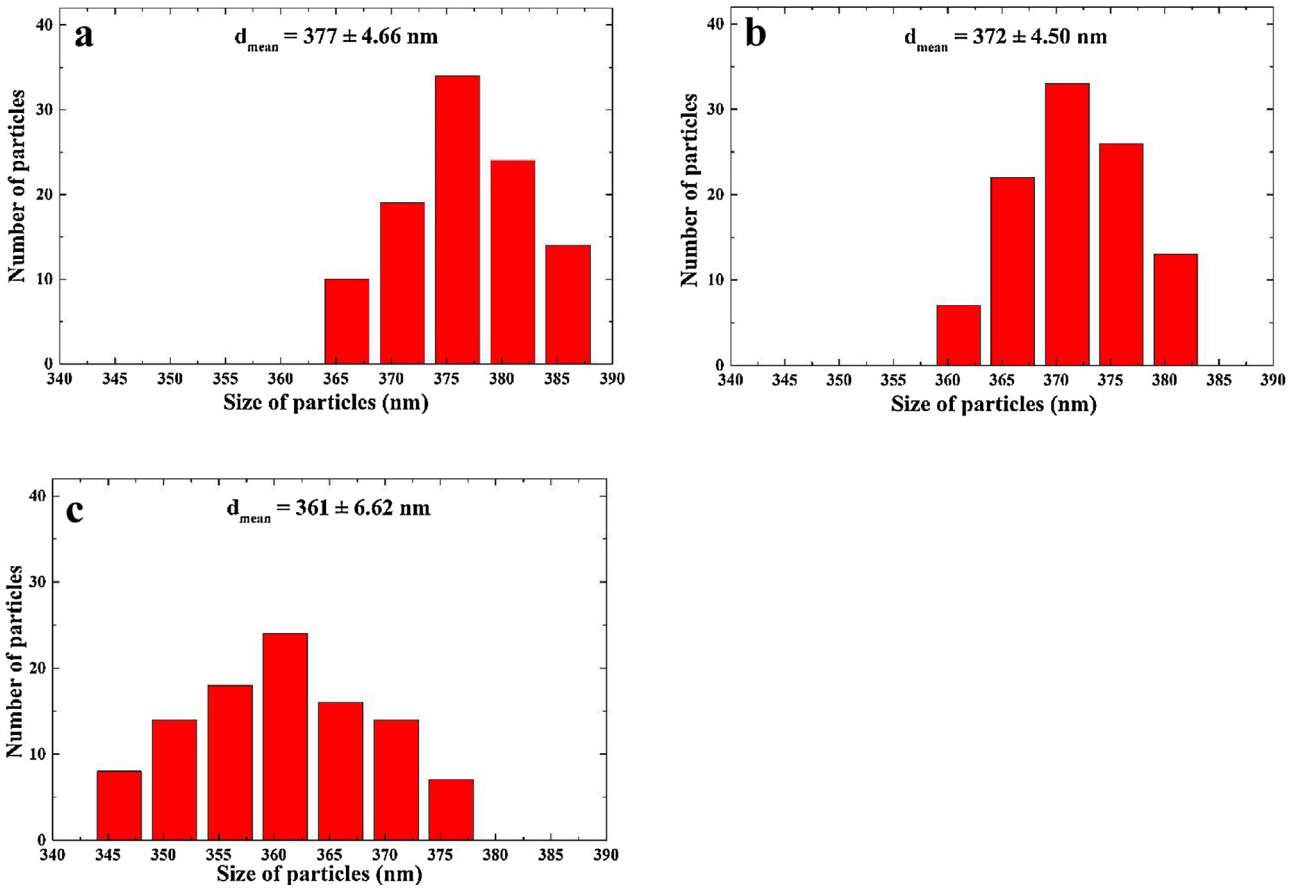

Fig. 3. Histogram of size dispersity of spheres for Sample 1 **(a)**, Sample 2 **(b)** and Sample 3 **(c)**.

Angle-resolved reflective measurements are represented in Fig. 4. Sample 1 shows reflectivity less than 4% as shown in Fig. 4a. The most interesting reflectivity is in Sample 2 (Fig. 4b) and Sample 3 (Fig. 4c). Sample 2 has shown reflectivity ~30% and Sample 3 has demonstrated ~74% reflectivity. The reflection maximum is observed at 12° and is attenuated with angel rise. An extra peak of reflection appears at about 70° for Sample 2.

Decreased intensity in Fig. 4 (from 4c to 4a) is observed because of the three samples available. Fig. 4a is the worst opal, with no order (see Fig. 2a). For this reason, it has the lowest reflectivity (less than 4%). Fig. 4b is a good opal with ~30% reflectivity (meniscus-like area corresponding Fig. 2b). Finally, Fig. 4c corresponds to Fig. 2c, demonstrating the best opal with perfectly-ordered spheres and maximum reflectivity. Thus, decreasing intensity is related to non-homogeneous assemblage of the opal.

We collected three reflectance spectra obtained at 14° in Fig. 4d for comparison. Fig. 4d shows that the peak of the maximum reflectivity of Sample 2 is shifted to the short-wave region relative to the maximum reflectivity peak for Sample 3.

The full width at half maximum (FWHM) was measured and the bandwidth ($\Delta\lambda/\lambda$) was estimated ~0.083 for Sample 3 (74% of reflectivity at 12° and λ_{max} = 866 nm). According to study [63], we have estimated the number of layers in Sample 3. The sample thickness with perfectly ordered spheres was estimated to be around 9 layers. The same result was turned out to visualize with SEM in cross-sections, ~9–11 layers.

Referring to Nair et al. [64,65], we measured spectrum at 56° for Sample 3 (see Fig. 5) and saw some peak splitting around 706 and 725 nm. Moreover, small diffraction peaks were also observed around 481, 524 and 599 nm. This could be explained by diffraction from different planes [66,67] of perfectly-ordered spheres.

For Sample 3, the reflectivity fetch was made as shown in Fig. 6a. It can be seen from Fig. 6a that there are several peaks in the short-wavelength region of the spectrum. The peaks are possibly related to the high-order PBG [68,69].

Maximum reflectivity values for the entire range of angles were selected as shown in Fig. 6b. It is worth noting that the Bruker spectrometer does not allow setting of the incident angle at less than 12°. For this reason, we made a fit for maximum reflectivity value dependence from angles for Sample 3. The curve of the fit allows estimation of the maximum reflectivity value at an angle less than 12°. As can be seen from Fig. 6b, maximum reflectivity becomes 98% at the 0° angle.

To estimate wavelength shift of maximum reflectivity from angle, we have built corresponding dependences for Sample 3 and Sample 2 as shown in Fig. 6c and d, respectively. Maximum reflectivity wavelength is seen in Fig. 6c–d to shift in longer wavelengths when the angle decreases. To analyse the wavelength of maximum reflectivity λ_{max} at 0° based on the Bragg-Snell law for angle-dependent diffraction, the effective refractive index n_{eff}, particle diameter D and fill factor f, a fit of dependences of maximum reflectivity wavelength from the angle was made. The equation has the following form [38,70]:

$$\lambda_{max} = d_{111}\sqrt{n_{eff}^2 - \sin^2\theta}, \quad (1)$$

where d_{111} is the inter-planar spacing between (111) planes and θ is the incident angle with respect to normal incidence. d_{111} is associated with particle diameter by the following equation:

$$d_{111} = D\sqrt{2/3}. \quad (2)$$

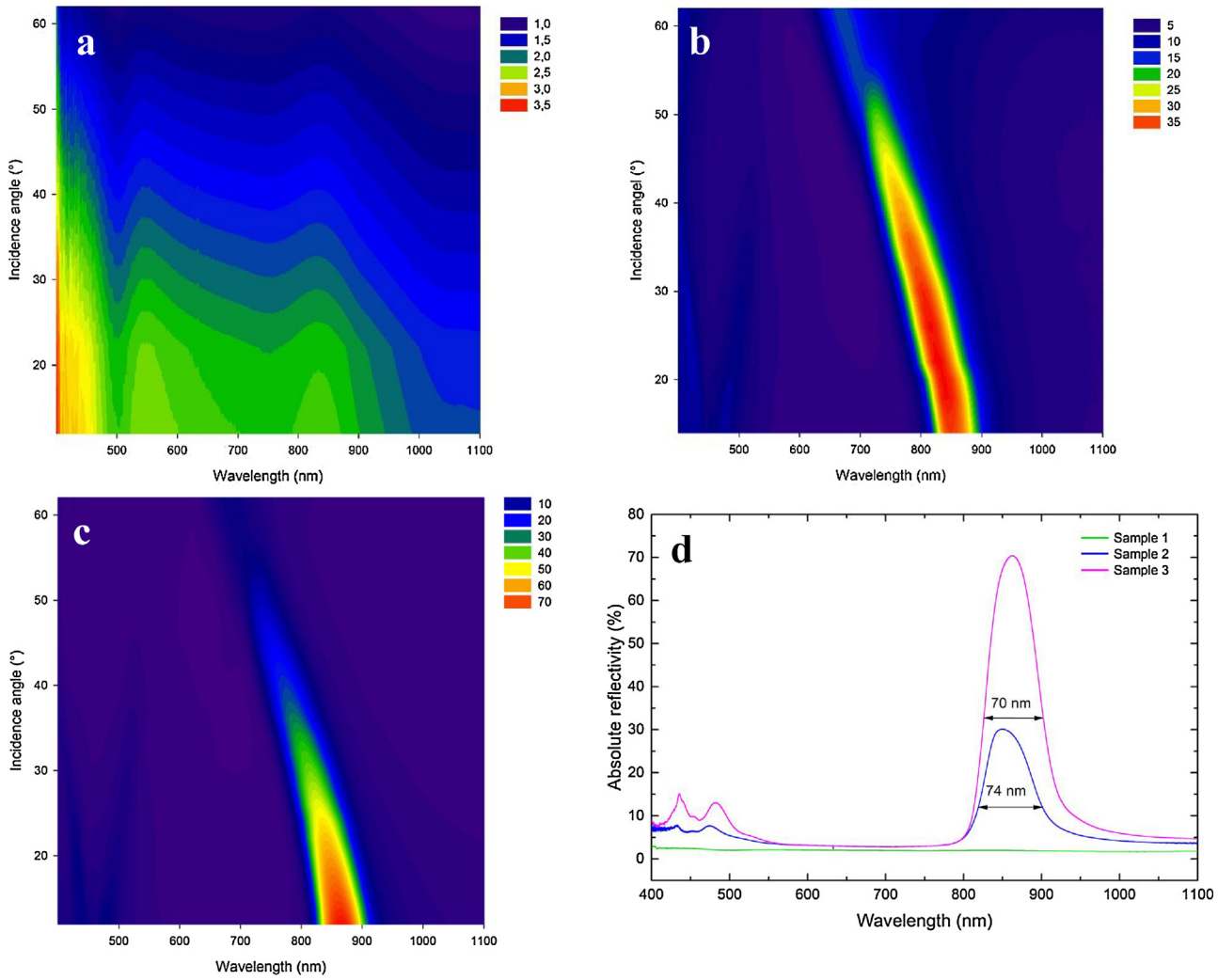

Fig. 4. Angular and spectral properties of absolute reflectivity for three different types of opal surface: Sample 1 (**a**), Sample 2 (**b**) and Sample 3 (**c**). Insets are absolute reflectivity in%. Absolute reflectivity spectra from three samples (Sample 1–3) measured at 14° (**d**).

In addition, n_{eff} is associated with fill factor by the following equation:

$$n_{eff}^2 = n_1^2 f + n_2^2 (1 - f), \quad (3)$$

where n_1 and n_2 is the refractive index for PMMA and air, respectively.

We have used n_{eff} and d_{111} as fitting parameters in Eq. (1). Fig. 6c–d shows the fit using Eq. (1) superimposed on the experimental data. The wavelength of maximum reflectivity λ_{max} at 0° was 869 nm for Sample 3 and 860 nm for Sample 2. The d_{111} was 303.76 and 306.46 for Sample 3 and Sample 2, respectively. Taking Eq. (2) into account, particle diameter D was 372 nm for Sample 3 and D was 375 nm for Sample 2. n_{eff} was 1.4304 and 1.4033 for Sample 3 and Sample 2, respectively. Since the refractive index of air is 1 and the refractive index of PMMA is 1.4833 (for 860 nm), and taking into consideration Eq. (3), f was 0.8715 for Sample 3 and 0.8075 for Sample 2.

The calculated filling factors are exceed the value of 0.74 for rigid spheres in the ideal defectless fcc lattice. However, PMMA spheres are sufficiently plastic and quite flexible, not hard and rigid. We believe that the particles are not in point contact with each other but are slightly pressed (partially flat wall contact but not point contact). It is confirmed by recent studies [55,56,62]. Thus there is a wide range of works [33,71,72] devoted to drying polymer films and declared that polymer particle deformation plays a crucial role.

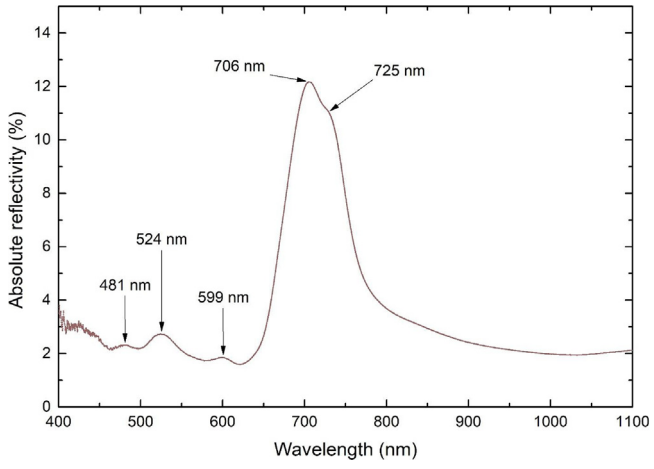

Fig. 5. Dependence of reflectivity from wavelength for Sample 3, measured at 56°.

That is probably a reason why the particles are packed more tightly than in the Gauss fcc model. It could also be taken into account for the high reflectivity. The obtained structural and optical parameters of the Samples 1–3 were collected in Table 1.

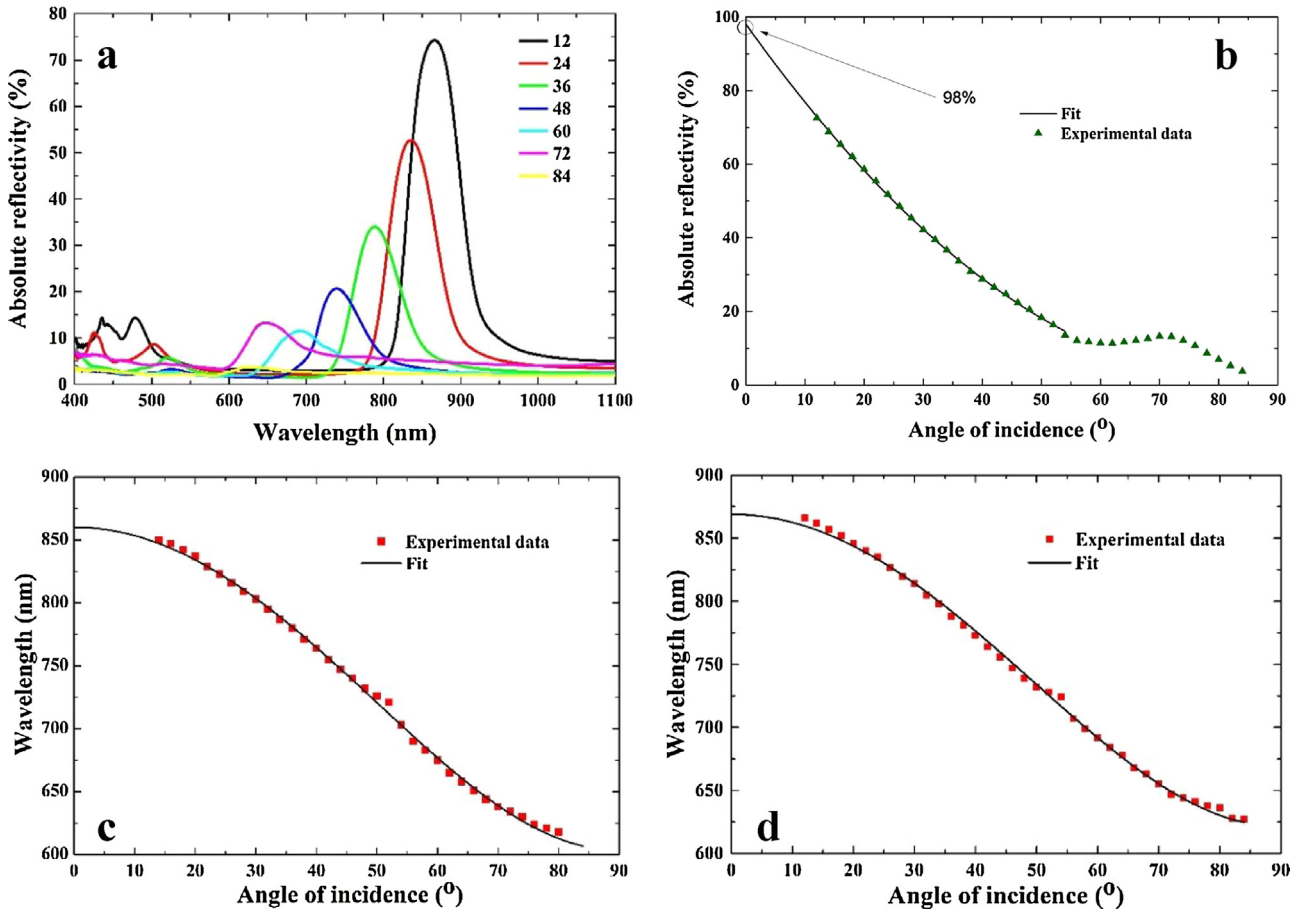

Fig. 6. The fetch of reflectivity for Sample 3, where the inset in the right top corner depicts the incident angle, ° (**a**). The dependence of maximum reflectivity from the angle for Sample 3, where red squares are experimental data and the solid line is a fit (**b**). The dependencies of maximum reflectivity wavelength from the angle for Sample 2 (**c**) and Sample 3 (**d**), where red squares are experimental data and the solid lines are the fits of Eq. (1). (For interpretation of the references to colour in this figure legend, the reader is referred to the web version of this article.)

Table 1
Parametric summary table of Sample 1–3.

Parameter	Sample 1	Sample 2	Sample 3
The place where it was taken from	bottom	meniscus	top
Mean diameter (determined with SEM), nm	377	372	361
Mean diameter (determined from spectra), nm	–	375	372
Filling factor	–	0.8075	0.8715
Absolute reflectivity at 14°, %	4	30	70
Absolute reflectivity at 12°, %	–	–	74
Extrapolated absolute reflectivity at 0°, %	–	–	98
FWHM at 14°, nm	–	74	70
$\Delta\lambda/\lambda$ at 14°	–	0.087	0.081

It should be noted that the particle diameter obtained by fitting Eq. (1) is in excellent agreement with the particle diameter obtained by SEM study. In addition, it can see that the reflectivity maximum significantly increases when the fill factor increases. Thus, we have obtained an opal PMMA crystal with a high-quality surface using a simple hybrid method.

4. Conclusion

We have prepared an opal PMMA crystal by a simple hybrid method. Three surfaces of this crystal were investigated by angle-resolved light reflection spectroscopy and by the SEM method. The angle-resolved reflective measurements were performed in the 400–1100 nm wavelength range.

The best surface of this crystal was found. The surface had narrow particle size distribution, with an average particle size of 361 nm. Most importantly, the extrapolated reflectivity of the surface reached 98% at normal light incidence. From angle-resolved reflective measurements, with the wavelength of maximum reflectivity at 0°, the particle diameter and the fill factor were determined using the fit of dependences of maximum reflectivity wavelength from the angle. The fit was based on the Bragg-Snell law. For the best surface, the extrapolated wavelength of maximum reflectivity at 0° was 869 nm. The particle diameter and fill factor were 372 nm and 0.8715, respectively. It was shown that the diameter obtained by fitting is in excellent agreement with the particle diameter obtained with SEM. Furthermore, the reflectivity maximum is demonstrated to increase significantly when the quality of lattice is improved. Other optical properties, for instance, luminescence properties may also be better in the case of high-quality PMMA opal crystal.

Thus, we believe that using our simple approach for manufacturing an opal PMMA crystal with a high-quality surface significantly increases the production of high-quality templates and thin films based on PhCs.

Acknowledgments

This study was supported by the Russian Foundation for Basic Research (Grant No. 16-32-00302 мол_а), by the Council for Grants of the President of the Russian Federation (SP-317.2015.1),

by Russian Foundation for Basic Research, Government of Krasnoyarsk Territory, Krasnoyarsk Region Science and Technology Support Fund to the research project No. 16-42-243059 р_мол_а and No. 16-48-242092 р_офи_м, and by the Program of Foundation for Promotion of Small Enterprises in Science and Technology (No.6662ГУ2015) ("УМНИК" program).

We acknowledge the support of Krasnoyarsk Regional Center for Collective Use of SB of RAS for equipment and technique. We thank A. V. Shabanov and O. V. Shabanova for assistance in dispersion preparation. We also thank V. G. Myagkov for useful discussion of the results.

References

[1] S.F. Joannopoulos, J.D. Pierre, R. Villeneuve, Photonic crystals:putting a new twist on light, Nature 386 (1997) 7, http://dx.doi.org/10.1038/386143a0.
[2] J.S. Skibina, R. Iliew, J. Bethge, M. Bock, D. Fischer, V.I. Beloglasov, R. Wedell, G. Steinmeyer, A chirped photonic-crystal fibre, Nat. Photonics 2 (2008), http://dx.doi.org/10.1038/nphoton.2008.203 (2008 211).
[3] H. Li, Z. Xu, B. Bao, N. Sun, Y. Song, Improving the luminescence performance of quantum dot-based photonic crystals for white-light emission, J. Mater. Chem. C 4 (2016) 39–44, http://dx.doi.org/10.1039/C5TC02428E.
[4] H. Kosaka, T. Kawashima, A. Tomita, M. Notomi, T. Tamamura, T. Sato, S. Kawakami, Photonic crystals for micro lightwave circuits using wavelength-dependent angular beam steering, Appl. Phys. Lett. 74 (1999), http://dx.doi.org/10.1063/1.123553.
[5] D. Zhou, D. Liu, W. Xu, X. Chen, Z. Yin, X. Bai, B. Dong, L. Xu, H. Song, Synergistic upconversion enhancement induced by multiple physical effects and an angle-dependent anticounterfeit application, Chem. Mater. 29 (2017) 6799–6809, http://dx.doi.org/10.1021/acs.chemmater.7b01783.
[6] W. Xu, Y. Zhu, X. Chen, J. Wang, L. Tao, S. Xu, T. Liu, H. Song, A novel strategy for improving upconversion luminescence of NaYF4:Yb, Er nanocrystals by coupling with hybrids of silver plasmon nanostructures and poly(methyl methacrylate) photonic crystals, Nano Res. 6 (2013) 795–807, http://dx.doi.org/10.1007/s12274-013-0358-y.
[7] D. Zhou, P. Zhou, D. Liu, W. Xu, Y. Zhu, S. Xu, Q. Dai, H. Song, Modulation of upconversion white light emission in PMMA/NaYF_4:Yb3+, Er3+, Tm3+ composite photonic crystals, Opt. Lett. 39 (2014) 4619, http://dx.doi.org/10.1364/OL.39.004619.
[8] H. Wang, Z. Yin, W. Xu, D. Zhou, S. Cui, X. Chen, H. Cui, H. Song, Remarkable enhancement of upconversion luminescence on 2-D anodic aluminum oxide photonic crystals, Nanoscale 8 (2016) 10004–10009, http://dx.doi.org/10.1039/C6NR00180G.
[9] A. Birner, R.B. Wehrspohn, U.M. Gösele, K. Busch, Silicon-based photonic crystals, Adv. Mater. 13 (2001) 377–388, http://dx.doi.org/10.1002/1521-4095(200103)13:6<377:AID-ADMA377>3.0.CO;2-X.
[10] E. Yablonovitch, Inhibited spontaneous emission in solid-state physics and electronics, Phys. Rev. Lett. 58 (1987) 2059–2062, http://dx.doi.org/10.1103/PhysRevLett.58.2059.
[11] E. Schonbrun, M. Abashin, J. Blair, Q. Wu, W. Park, Y. Fainman, C.J. Summers, Total internal reflection photonic crystal prism, Opt. Express 15 (2007) 8065, http://dx.doi.org/10.1364/OE.15.008065.
[12] C. Bouzigues, T. Gacoin, A. Alexandrou, Biological applications of rare-earth based nanoparticles, ACS Nano 5 (2011) 8488–8505, http://dx.doi.org/10.1021/nn202378b.
[13] Q. Liu, T. Yang, W. Feng, F. Li, Blue-emissive upconversion nanoparticles for low-power-excited bioimaging in vivo, J. Am. Chem. Soc. 134 (2012) 5390–5397, http://dx.doi.org/10.1021/ja3003638.
[14] Highly efficient lanthanide upconverting nanomaterials: progresses and challenges, Nano Today 8 (2013) 643–676, http://dx.doi.org/10.1016/J.NANTOD.2013.11.003.
[15] Y. Liu, D. Tu, H. Zhu, X. Chen, Lanthanide-doped luminescent nanoprobes: controlled synthesis, optical spectroscopy, and bioapplications, Chem. Soc. Rev. 42 (2013) 6924, http://dx.doi.org/10.1039/c3cs60060b.
[16] M. Nyk, R. Kumar, T.Y. Ohulchanskyy, E.J. Bergey, P.N. Prasad, High contrast in vitro and in vivo photoluminescence bioimaging using near infrared to near infrared up-conversion in Tm 3+ and Yb 3+ doped fluoride nanophosphors, Nano Lett. 8 (2008) 3834–3838, http://dx.doi.org/10.1021/nl802223f.
[17] X. Huang, S. Han, W. Huang, X. Liu, Enhancing solar cell efficiency: the search for luminescent materials as spectral converters, Chem. Soc. Rev. 42 (2013) 173–201, http://dx.doi.org/10.1039/c2cs35288e.
[18] H.-Q. Wang, M. Batentschuk, A. Osvet, L. Pinna, C.J. Brabec, Rare-earth ion doped up-conversion materials for photovoltaic applications, Adv. Mater. 23 (2011) 2675–2680, http://dx.doi.org/10.1002/adma.201100511.
[19] S.Y. Lin, J.G. Fleming, D.L. Hetherington, B.K. Smith, R. Biswas, K.M. Ho, M.M. Sigalas, W. Zubrzycki, S.R. Kurtz, J. Bur, A three-dimensional photonic crystal operating at infrared wavelengths, Nature 394 (1998) 251–253, http://dx.doi.org/10.1038/28343.
[20] O. Glushko, R. Brunner, R. Meisels, S. Kalchmair, G. Strasser, Extraordinary transmission in metal hole array-photonic crystal hybrid structures, Opt. Express 20 (2012) 17174, http://dx.doi.org/10.1364/OE.20.017174.
[21] M.D. Nielsen, C. Jacobsen, N.A. Mortensen, J.R. Folkenberg, H.R. Simonsen, Low-loss photonic crystal fibers for transmission systems and their dispersion properties, Opt. Express 12 (2004) 1372, http://dx.doi.org/10.1364/OPEX.12.001372.
[22] L. Zeng, P. Bermel, Y. Yi, B.A. Alamariu, K.A. Broderick, J. Liu, C. Hong, X. Duan, J. Joannopoulos, L.C. Kimerling, Demonstration of enhanced absorption in thin film Si solar cells with textured photonic crystal back reflector, Appl. Phys. Lett. 93 (2008) 221105, http://dx.doi.org/10.1063/1.3039787.
[23] Suzushi Nishimura, Neal Abrams, Bradley A. Lewis, Lara I. Halaoui, Thomas E. Mallouk, Kurt D. Benkstein, Jao van de Lagemaat, A.J. Frank, Standing wave enhancement of red absorbance and photocurrent in dye-sensitized titanium dioxide photoelectrodes coupled to photonic crystals, J. Am. Chem. Soc. 125 (20) (2003) 6306–6310, http://dx.doi.org/10.1021/JA034650P.
[24] H. Wang, X. Gu, R. Hu, J.W.Y. Lam, D. Zhang, B.Z. Tang, J. van de Lagemaat, A.J. Frank, Y.-P. Li, Y.-G. Ma, H.-B. Sun, D. Zhang, D. Wiersma, G.A. Ozin, Luminescent photonic crystals with multi-functionality and tunability, Chem. Sci. 7 (2016) 5692–5698, http://dx.doi.org/10.1039/C6SC01703G.
[25] J.C. Knight, Photonic crystal fibres, Nature 424 (2003) 847–851, http://dx.doi.org/10.1038/nature01940.
[26] G. Shambat, B. Ellis, A. Majumdar, J. Petykiewicz, M.A. Mayer, T. Sarmiento, J. Harris, E.E. Haller, J. Vučković, Ultrafast direct modulation of a single-mode photonic crystal nanocavity light-emitting diode, Nat. Commun. 2 (2011) 539, http://dx.doi.org/10.1038/ncomms1543.
[27] S.-P. Yu, J.D. Hood, J.A. Muniz, M.J. Martin, R. Norte, C.-L. Hung, S.M. Meenehan, J.D. Cohen, O. Painter, H.J. Kimble, Nanowire photonic crystal waveguides for single-atom trapping and strong light-matter interactions, Appl. Phys. Lett. 104 (2014) 111103, http://dx.doi.org/10.1063/1.4868975.
[28] S. Pleasants, Photonic-crystal waveguides: trapping single atoms, Nat. Photonics 8 (2014), http://dx.doi.org/10.1038/nphoton.2014.131, 427–427.
[29] W.J. Otter, S.M. Hanham, N.M. Ridler, G. Marino, N. Klein, S. Lucyszyn, 100 GHz ultra-high Q-factor photonic crystal resonators, Sens. Actuators A Phys. 217 (2014) 151–159, http://dx.doi.org/10.1016/j.sna.2014.06.022.
[30] Y. Zhang, M. Khan, Y. Huang, J. Ryou, P. Deotare, R. Dupuis, M. Lončar, Photonic crystal nanobeam lasers, Appl. Phys. Lett. 97 (2010) 51104, http://dx.doi.org/10.1063/1.3475397.
[31] J. Zhang, Z. Sun, B. Yang, Self-assembly of photonic crystals from polymer colloids, Curr. Opin. Colloid. Interface Sci. 14 (2009) 103–114, http://dx.doi.org/10.1016/j.cocis.2008.09.001.
[32] C.E. Finlayson, J.J. Baumberg, Generating bulk-scale ordered optical materials using shear-assembly in viscoelastic media, Mater 10 (2017) 688, http://dx.doi.org/10.3390/ma10070688.
[33] Q. Zhao, C.E. Finlayson, C.G. Schaefer, P. Spahn, M. Gallei, L. Herrmann, A.V. Petukhov, J.J. Baumberg, Nanoassembly of polydisperse photonic crystals based on binary and ternary polymer opal alloys, Adv. Opt. Mater. 4 (2016) 1494–1500, http://dx.doi.org/10.1002/adom.201600328.
[34] J. Ge, Y. Yin, Responsive photonic crystals, Angew. Chemie Int. Ed. 50 (2011) 1492–1522, http://dx.doi.org/10.1002/anie.200907091.
[35] D. Scheid, C. Lederle, S. Vowinkel, C.G. Schäfer, B. Stühn, M. Gallei, Redox- and mechano-chromic response of metallopolymer-based elastomeric colloidal crystal films, J. Mater. Chem. C 2 (2014) 2583, http://dx.doi.org/10.1039/c3tc32525c.
[36] J.-H. Lee, C.Y. Koh, J.P. Singer, S.-J. Jeon, M. Maldovan, O. Stein, E.L. Thomas, 25th anniversary article: ordered polymer structures for the engineering of photons and phonons, Adv. Mater. 26 (2014) 532–569, http://dx.doi.org/10.1002/adma.201303456.
[37] C.G. Schäfer, M. Gallei, J.T. Zahn, J. Engelhardt, G.P. Hellmann, M. Rehahn, Reversible light-, thermo-, and mechano-responsive elastomeric polymer opal films, Chem. Mater. 25 (2013) 2309–2318, http://dx.doi.org/10.1021/cm400911j.
[38] E. Armstrong, C. O'Dwyer, Artificial opal photonic crystals and inverse opal structures –fundamentals and applications from optics to energy storage, J. Mater. Chem. C 3 (2015) 6109–6143, http://dx.doi.org/10.1039/C5TC01083G.
[39] G.I.N. Waterhouse, M.R. Waterland, Opal and inverse opal photonic crystals: fabrication and characterization, Polyhedron 26 (2007) 356–368, http://dx.doi.org/10.1016/j.poly.2006.06.024.
[40] S. Kedia, R. Vijaya, A.K. Ray, S. Sinha, Photonic stop band effect in ZnO inverse photonic crystal, Opt. Mater. (Amst.) 33 (2011) 466–474, http://dx.doi.org/10.1016/j.optmat.2010.10.020.
[41] W.-K. Kuo, H.-P. Weng, J.-J. Hsu, H. Yu, Photonic crystal-based sensors for detecting alcohol concentration, Appl. Sci. 6 (2016) 67, http://dx.doi.org/10.3390/app6030067.
[42] C.S. Lee, Z. Dai, S.Y. Jeong, C.H. Kwak, B.Y. Kim, D.H. Kim, H.W. Jang, J.S. Park, J.H. Lee, Monolayer Co3O4 inverse opals as multifunctional sensors for volatile organic compounds, Chem. A Eur. J. 22 (2016) 7102–7107, http://dx.doi.org/10.1002/chem.201505210.
[43] Y. Zhu, S. Cui, Y. Wang, M. Liu, C. Lu, A. Mishra, W. Xu, Enhanced rare earth photoluminescence in inverse opal photonic crystals and its application for pH sensing, Nanotechnology 27 (2016) 405202, http://dx.doi.org/10.1088/0957-4484/27/40/405202.
[44] K.T. Lee, J.C. Lytle, N.S. Ergang, S.M. Oh, A. Stein, Synthesis and rate performance of monolithic macroporous carbon electrodes for lithium-ion secondary batteries, Adv. Funct. Mater. 15 (2005) 547–556, http://dx.doi.org/10.1002/adfm.200400186.
[45] M.A. Al-Daous, A. Stein, Preparation and catalytic evaluation of macroporous crystalline sulfated zirconium dioxide templated with colloidal crystals, Chem. Mater. 15 (2003) 2638–2645, http://dx.doi.org/10.1021/cm030019b.

[46] I.K. Sung, A. Christian, M. Mitchell, D.P. Kim, P.J.A. Kenis, Tailored macroporous SiCN and SiC structures for high-temperature fuel reforming, Adv. Funct. Mater. 15 (2005) 1336–1342, http://dx.doi.org/10.1002/adfm.200500038.
[47] M.-Y. Tsang, N.E. Pridmore, L.J. Gillie, Y.-H. Chou, R. Brydson, R.E. Douthwaite, Enhanced photocatalytic hydrogen generation using polymorphic macroporous TaON, Adv. Mater. 24 (2012) 3406–3409, http://dx.doi.org/10.1002/adma.201201193.
[48] C.G. Schäfer, T. Winter, S. Heidt, C. Dietz, T. Ding, J.J. Baumberg, M. Gallei, Smart polymer inverse-opal photonic crystal films by melt-shear organization for hybrid core?shell architectures, J. Mater. Chem. C 3 (2015) 2204–2214, http://dx.doi.org/10.1039/C4TC02788D.
[49] D.P. Puzzo, A.C. Arsenault, I. Manners, G.A. Ozin, Electroactive inverse opal: a single material for all colors, Angew. Chemie Int. Ed. 48 (2009) 943–947, http://dx.doi.org/10.1002/anie.200804391.
[50] C. Fenzl, T. Hirsch, O.S. Wolfbeis, Photonic crystals for chemical sensing and biosensing, Angew. Chemie Int. Ed. 53 (2014) 3318–3335, http://dx.doi.org/10.1002/anie.201307828.
[51] N. Tétreault, H. Míguez, G.A. Ozin, Silicon inverse Opal—A platform for photonic bandgap research, Adv. Mater. 16 (2004) 1471–1476, http://dx.doi.org/10.1002/adma.200400618.
[52] G. Lozano, H. Míguez, Relation between growth dynamics and the spatial distribution of intrinsic defects in self-assembled colloidal crystal films, Appl. Phys. Lett. 92 (2008) 91904, http://dx.doi.org/10.1063/1.2883943.
[53] E. Palacios-Lidón, B.H. Juárez, E. Castillo-Martínez, C. López, Optical and morphological study of disorder in opals, J. Appl. Phys. 97 (2005) 63502, http://dx.doi.org/10.1063/1.1851014.
[54] E. Palacios, Heat-resistant PMMA photonic crystal films with bright structural color, Dye. Pigment. 99 (2013) 1022–1028, http://dx.doi.org/10.1016/J.DYEPIG.2013.08.012.
[55] Y. Huang, J. Zhou, B. Su, L. Shi, J. Wang, S. Chen, L. Wang, J. Zi, Y. Song, L. Jiang, Colloidal photonic crystals with narrow stopbands assembled from low-adhesive superhydrophobic substrates, J. Am. Chem. Soc. 134 (2012) 17053–17058, http://dx.doi.org/10.1021/ja304751k.
[56] T. Xia, W. Luo, F. Hu, W. Qiu, Z. Zhang, Y. Lin, X.Y. Liu, Fabrication of crack-free photonic crystal films on superhydrophobic nanopin surface, ACS Appl. Mater. Interfaces 9 (2017) 22037–22041, http://dx.doi.org/10.1021/acsami.7b04653.
[57] O.V. Shabanova, M.A. Korshunov, I.V. Nemtsev, A.V. Shabanov, Features of self-assembly of opal-like structures based on poly(methyl methacrylate) submicron dispersions, Nanotechnol. Russ. 11 (2016), http://dx.doi.org/10.1134/S1995078016050153.
[58] B. Kaczmarczyk, B. Morejko-Buz, A. Stolarzewicz, Investigation of infrared calibration methods for application to the study of methyl methacrylate polymerization, Fresenius. J. Anal. Chem. 370 (2001) 899–903 (Accessed October 18, 2017) http://www.ncbi.nlm.nih.gov/pubmed/11569872.
[59] I. Lipschitz, The vibrational spectrum of Poly(Methyl methacrylate): a review, Polym. Plast. Technol. Eng. 19 (1982) 53–106, http://dx.doi.org/10.1080/03602558208067727.
[60] P. Sutandar, D.J. Ahn, E.I. Franses, FTIR ATR analysis for microstructure and water uptake in poly(methyl methacrylate) spin cast and Langmuir-Blodgett thin films, Macromolecules 27 (1994) 7316–7328, http://dx.doi.org/10.1021/ma00103a013.
[61] P. Jiang, J.F. Bertone, K.S. Hwang, V.L. Colvin, Single-crystal colloidal multilayers of controlled thickness, Chem. Mater. 11 (1999) 2132–2140, http://dx.doi.org/10.1021/cm990080+.
[62] J.-H. Yoo, H.-J. Kwon, D. Paeng, J. Yeo, S. Elhadj, C.P. Grigoropoulos, Facile fabrication of a superhydrophobic cage by laser direct writing for site-specific colloidal self-assembled photonic crystal, Nanotechnology 27 (2016) 145604, http://dx.doi.org/10.1088/0957-4484/27/14/145604.
[63] J.F. Galisteo, F. García-Santamaría, D. Golmayo, B.H. Juárez, C. López, E. Palacios, Self-assembly approach to optical metamaterials, J. Opt. A Pure Appl. Opt. 7 (2005) S244–S254, http://dx.doi.org/10.1088/1464-4258/7/2/033.
[64] R.V. Nair, B.N. Jagatap, Multiple Bragg diffraction at W point in the face centered cubic photonic crystals, J. Nanophotonics 9 (2015) 93076, http://dx.doi.org/10.1117/1.JNP.9.093076.
[65] Priya, R.V. Nair, Polarization-selective branching of stop gaps in three-dimensional photonic crystals, Phys. Rev. A 93 (2016), http://dx.doi.org/10.1103/PhysRevA.93.063850.
[66] C.G. Schäfer, D.A. Smolin, G.P. Hellmann, M. Gallei, Fully reversible shape transition of soft spheres in elastomeric polymer opal films, Langmuir 29 (2013) 11275–11283, http://dx.doi.org/10.1021/la4023695.
[67] I. Maurin, E. Moufarej, A. Laliotis, D. Bloch, Optics of an Opal Modeled with a Stratified Effective Index and the Effect of the Interface, 2015, http://arxiv.org/abs/1507.08548 (Accessed October 19, 2017).
[68] W. Xu, X. Bai, Y. Zhu, T. Liu, S. Xu, B. Dong, H. Song, Communication Excitation band modulation with high-order photonic band gap in PMMA:Eu(TTA) 3 (TPPO) 2 opals, J. Chem. Phys. 138 (2013) 181103, http://dx.doi.org/10.1063/1.4804980.
[69] R.V. Nair, R. Vijaya, Observation of higher-order diffraction features in self-assembled photonic crystals, Phys. Rev. A 76 (2007) 53805, http://dx.doi.org/10.1103/PhysRevA.76.053805.
[70] K. Liu, T.A. Schmedake, R. Tsu, A comparative study of colloidal silica spheres: photonic crystals versus Bragg's law, Phys. Lett. A 372 (2008) 4517–4520, http://dx.doi.org/10.1016/j.physleta.2008.04.008.
[71] Q. Zhao, C.E. Finlayson, D.R.E. Snoswell, A. Haines, C. Schäfer, P. Spahn, G.P. Hellmann, A.V. Petukhov, L. Herrmann, P. Burdet, P.A. Midgley, S. Butler, M. Mackley, Q. Guo, J.J. Baumberg, Large-scale ordering of nanoparticles using viscoelastic shear processing, Nat. Commun. 7 (2016) 11661, http://dx.doi.org/10.1038/ncomms11661.
[72] M. Visschers, J. Laven, A.L. German, Current understanding of the deformation of latex particles during film formation, Prog. Org. Coat. 30 (1997) 39–49, http://dx.doi.org/10.1016/S0300-9440(96)00652-2.